Structural and Photoluminescence Properties of Excited State Intramolecular Proton Transfer Capable Compounds—Potential Emissive and Electron Transport Materials

Alexander V. Gaenko,*,†,‡ Ajitha Devarajan,† Igor V. Tselinskii,‡ and Ulf Ryde†

Department of Theoretical Chemistry, Chemical Center, Lund University, P.O. Box 124, S-221 00 Lund, Sweden, and St. Petersburg State Institute of Technology (Technical University), Moskovskii av. 26, 190013 St. Petersburg, Russia

Received: January 30, 2006; In Final Form: April 14, 2006

Electronic factors influencing the photoluminescence properties and rates of excited state intramolecular proton transfer (ESIPT) reaction of *o*-hydroxy derivatives of 2,5-diphenyl-1,3,4-oxadiazole have been studied. The potential of these molecules as emissive and electron transport materials in designing improved organic light emitting diodes (OLEDs) has been studied by analyzing possible reasons for the unusually high Stokes shifts and ESIPT reaction rates. Time-dependent density functional theory (TDDFT) methods have been used to calculate the ground and excited state properties of the phototautomers that are the ESIPT reaction products. We study the relative effect of electron-withdrawing substituents on the proton-acceptor moiety and predict that the lowest ESIPT rate (1.9×10^{11} s^{-1}) is achieved with a dimethylamino substituent and that the Stokes shifts are around 11 000 cm^{-1} for all three derivatives.

1. Introduction

ESIPT is observed in a wide range of organic molecules. Organic luminophores that undergo ESIPT are usually characterized by abnormally large fluorescence Stokes shifts.[1,2] This effect finds its application in many areas: Materials showing high fluorescence Stokes shifts are used in high-energy radiation detectors.[3,4] In fluorescent analysis of biological systems,[5] a large Stokes shift is favorable because it corresponds better to the spectral region of less light absorption of biomaterials.[6] The inverse population of the energy states due to ESIPT leads to the use of the effect in chemical lasers.[7] As the ESIPT process often results in a noticeable quenching of fluorescence,[1,8] substances exhibiting ESIPT reaction can be used as UV photostabilizers.[9,10]

Organic luminophores capable of ESIPT have the potential to be construction materials for electroluminescence devices (organic light emitting diodes, OLEDs).[2] The main advantage of the large Stokes shifts is the increase in light output as a result of a low self-absorption of the emitted light.[11] On the other hand, the often-observed fluorescence quenching may result in a decrease of OLED efficiency.

The requirement for an organic molecule to be capable of ESIPT is the presence of a proton-donor moiety and a proton-acceptor moiety in close proximity (less than 2 Å), sharing an intramolecular hydrogen bond and in direct polar conjugation.[8,2] Typically, the proton-donor site is an amino or hydroxyl group.

o-Hydroxy derivatives of 2,5-diphenyl-1,3,4-oxadiazoles are ideal model compounds for studying the effect of substituents on the fluorescence properties, because the proton-donor and -acceptor parts are clearly separated.[8] Moreover, the 1,3,4-oxadiazole moiety is known for its high electron affinity and substances containing an oxadiazole fragment (both low-molecular-weight and polymers) are promising materials for the constructing of OLEDs,[12] both as electron-transporting and hole-blocking layers[13−19] and as light-emission layers.[20,21]

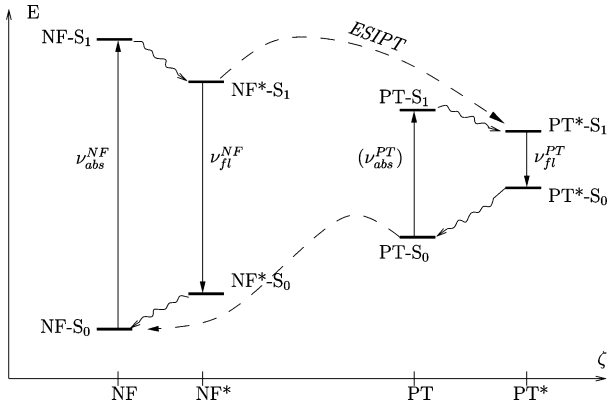

Figure 1. Energy diagram of the phototautomerization.

In the past few years, with the development of variational formulation[22] of time-dependent (TD) density functional theory (DFT), considerable progress has been achieved in calculation of excited state molecular properties. Although a number of high-quality studies of ESIPT process in a series of molecular systems have been published,[23−25] to the best of authors' knowledge no investigations of the ESIPT process in 1,3,4-oxadiazole derivatives at reasonable level have been presented.

Experimental studies by Doroshenko[8] on the substituent effects on the fluorescence properties of several derivatives of these compounds revealed that the fluorescence properties can be tuned from a complete quenching of the phototautomer emission up to a considerable quantum yield with the introduction of electron-accepting substituents either in the proton-accepting or in the proton-donor moieties.

A generalized scheme of the primary photophysical and photochemical processes that act in the excited state for molecules capable of ESIPT is presented in Figure 1.[2,8]

Initially, the molecule is in its ground state, the "normal form" NF-S_0. Upon photoexcitation, the molecule is vertically excited

† Lund University.
‡ St. Petersburg State Institute of Technology (Technical University).

10.1021/jp060646z CCC: $33.50 © 2006 American Chemical Society
Published on Web 06/06/2006

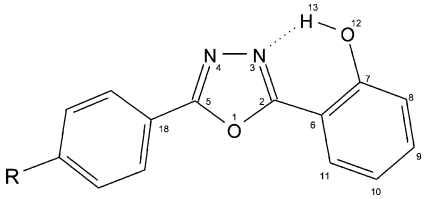

$$R = (CH_3)_2N\ ,\quad CH_3O,\quad Ph$$

Figure 2. Normal form.

to the first excited singlet state NF-S_1 with the energy difference corresponding to the most intensive peak in the absorption spectrum. From this Franck−Condon excited state, the molecular geometry may relax to the minimum of the first excited state (NF*-S_1) and undergo a tautomerization via ESIPT to the excited state (PT*-S_1). Tautomerization via ESIPT directly from NF-S_1 to PT*-S_1 is also possible. From the excited state phototautomer (PT*-S_1), the molecule may emit a photon and fall to the ground state phototautomer (PT*-S_0) with the energy difference corresponding to the peak in the fluorescence spectrum.

We will use the following terms to describe the chemical structures, geometries and electronic states in question:

•NF−S_0, NF−S_1: ground and the first excited singlet states of the normal form, respectively, at the ground state optimized geometry

•NF*-S_0, NF*-S_1: ground and the first excited singlet states of the normal form, respectively, at the first excited singlet state optimized geometry

•PT-S_0, PT-S_1: ground and the first excited singlet states of the phototautomeric form, respectively, at the ground state optimized geometry

•PT*-S_0, PT*-S_1: ground and the first excited singlet states of the phototautomeric form, respectively, at the first excited singlet state optimized geometry

In the present investigation we have optimized the structures of the ground and excited states of the normal and phototautomeric forms of these molecules at the correlated level and we have calculated the absorption and fluorescent properties. Effects of electron-accepting and electron-donor substituents on the proton-accepting moiety have been analyzed. We compare our results with those of earlier theoretical calculations at the semiempirical level.[1,8]

The present paper is organized as follows: In section 2, we describe briefly the computational details, including basis set and structural formula for normal and tautomeric forms. We also briefly describe the procedure used to calculate the spectral properties. In section 3, we present the results and discuss the spectra, the electron density distribution in ground and excited states, relative ESIPT reaction rates and fluorescent properties for the *o*-hydroxy-2,5-diphenyl-1,3,4-oxadiazole derivatives. A Summary and Conclusions are presented in section 4.

2. Computational Details

In this paper, we study three substituted *o*-hydroxy-2,5-diphenyl-1,3,4-oxadiazoles with the substituents being *N*,*N*′-dimethylamino, methoxy, or a phenyl group. The structure of their normal and tautomeric forms are shown in Figures 2 and 3, respectively, with the enumeration of the atoms used in the present paper.

The 2-phenyl ring ("right") acts as a proton-donor moiety and the oxadiazole ring with the 5-phenyl ring ("left") act as a proton-acceptor moiety. The hydrogen from the *o*-hydroxy group on the 2-phenyl ring forms a hydrogen bond with the proximal nitrogen of the oxadiazole ring. The tautomeric structure can in principle exist either in a zwitterionic or in a quinoid form (Figure 3).

The three substituents form a series of decreasing electron-donating character ($(CH_3)_2N$ < CH_3O < Ph). The *N*,*N*′-dimethylamino derivative, along with the electron-transporting 1,3,4-oxadiazole fragment, also has a hole-transporting dimethylamino group. This combination makes this substance a potential candidate for emitter-layer material[12] in OLED devices.

The ground state geometries of the normal forms (NF) of the *o*-hydroxy derivatives of 2,5-diphenyl-1,3,4-oxadiazole were optimized without any symmetry constraints at the DFT level[26] using the B3LYP functional.[27−29] We have used the TZVP basis[30,31] for all atoms. Absorption spectra are calculated by the TDDFT method.[32−34] We have calculated 35 low-lying singlet states. The lowest excitation energy at this geometry corresponds to the absorption frequency (ν_{abs}^{NF}).

To calculate the fluorescence properties, the geometry of the first excited singlet state of the normal form (NF*-S_1) was optimized using TDDFT method.[22] The energy difference between the first excited state at this geometry and the ground state at its optimum geometry corresponds to the adiabatic excitation energy. The energy difference between the ground and first excited state at the excited state geometry corresponds to the emission frequency of the normal form (ν_{fl}^{NF}). Stokes shifts are calculated as differences between the emission and absorption frequencies. A similar procedure was carried out for determining the ground state of phototautomeric forms (PT-S_0) and the first excited state of phototautomeric form (PT*-S_1).

For all three substituents, the ESIPT reaction paths were evaluated by means of constrained optimization (coordinate-driven minimum energy path approach[24,35,36]). For a series of fixed O(12)−H(13) bond lengths, the other geometry parameters were optimized. The transition states energies and geometries were estimated as the maxima of these potential energy surface cross-sections.

To study changes in the electron density distribution between the ground state and vertical and adiabatic excited states of normal and phototautomeric forms, we analyzed the dipole moments and Mulliken charges of the ground and excited states of both tautomers. The leading orbital transitions contributing to the excited states are also reported.

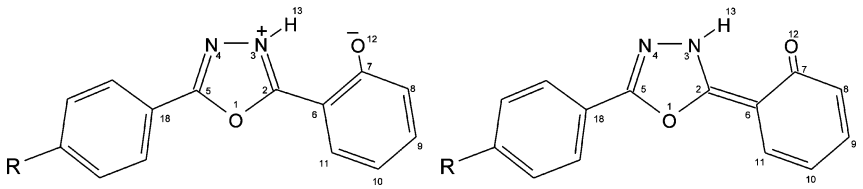

$$R = (CH_3)_2N,\quad CH_3O,\quad Ph$$

Figure 3. Zwitterionic and quinoid form of the phototautomer.

TABLE 1: Selected Bond Lengths

bond	R = $(CH_3)_2N$				R = CH_3O				R = Ph			
O1C2	1.361	1.382	1.312	1.355	1.361	1.376	1.310	1.356	1.360	1.364	1.310	1.356
C2N3	1.301	1.358	1.289	1.331	1.302	1.341	1.289	1.333	1.303	1.318	1.291	1.334
N3N4	1.386	1.343	1.393	1.372	1.385	1.329	1.399	1.370	1.384	1.341	1.402	1.368
N4C5	1.298	1.313	1.362	1.294	1.296	1.345	1.357	1.292	1.295	1.347	1.342	1.291
O1C5	1.376	1.385	1.442	1.389	1.374	1.392	1.439	1.387	1.374	1.393	1.430	1.386
C2C6	1.444	1.400	1.473	1.397	1.443	1.409	1.474	1.395	1.443	1.426	1.469	1.394
C5C18	1.447	1.428	1.389	1.444	1.451	1.409	1.393	1.448	1.453	1.403	1.397	1.450
C7O12	1.345	1.349	1.257	1.264	1.345	1.331	1.257	1.263	1.345	1.322	1.256	1.263
O12H13	0.986	0.987	2.058	1.774	0.986	1.000	2.057	1.768	0.985	1.007	2.052	1.768
N3H13	1.803	1.798	1.015	1.035	1.807	1.740	1.014	1.036	1.812	1.707	1.015	1.036
C6C7	1.416	1.442	1.454	1.462	1.416	1.451	1.453	1.463	1.416	1.447	1.454	1.463
C7C8	1.398	1.387	1.440	1.440	1.398	1.397	1.440	1.440	1.398	1.405	1.440	1.440
C8C9	1.384	1.399	1.385	1.367	1.384	1.388	1.385	1.367	1.384	1.380	1.384	1.366
C9C10	1.398	1.403	1.389	1.421	1.398	1.407	1.389	1.421	1.398	1.408	1.390	1.422
C10C11	1.383	1.379	1.367	1.367	1.382	1.384	1.367	1.367	1.382	1.388	1.369	1.366
C11C6	1.403	1.430	1.367	1.419	1.404	1.414	1.367	1.420	1.404	1.400	1.369	1.421

For all calculations, we have used the TURBOMOLE 5.7[37] suite of programs.

3. Results and Discussion

3.1. Geometry. The molecules are planar (C_s symmetry) with the exception of the phenyl derivative. In the latter molecule, the angle between phenyl ring planes in the substituent is 39° in the ground state normal form (NF-S_0) and becomes 22° in excited state (NF*-S_1). Likewise, in the (excited) phototautomeric form (PT*-S_1), the angle is 26° and it becomes 39° in the ground state tautomeric form (PT-S_0).

The lengths of the most significantly changed bonds are presented in Table 1. One can see that bond lengths are consistent with the single/double character implied by corresponding structural formulas. It is not possible to decide the character of the phototautomers: The short C(2)−N(3) and the long C(2)−C(6) bonds point toward the zwitterionic form, but the short C(7)−O(12) bond and the long C(7)−C(6) and C(7)−C(8) bonds are more in accordance with the quinoid form. Changes in the bond lengths in the excited molecules with respect to their ground state geometries (double bonds become longer, single bonds become shorter) can be ascribed to changes in bond orders and are consistent with the electron density redistributions.

3.2. UV/Vis Absorption Spectra. Absorption spectra of the normal forms of the substituted *o*-hydroxy derivatives of 2,5-diphenyl-1,3,4-oxadiazole were calculated with the TDDFT method. Excitation energies of the 35 lowest singlets were calculated and the 10 lowest ones with oscillator strengths higher than 0.01 are tabulated and can be found in the Supporting Information. In all cases, the most intense peak corresponds to the excitation to the first singlet excited state ($S_0 \rightarrow S_1$), which is mainly a HOMO to LUMO electronic transition.

The corresponding results for the tautomeric forms are also tabulated in Supporting Information. The spectra of both forms are represented graphically in Figures 4 and 5, in which the shape of each spectral line is approximated by Gaussian function (FWHM = 5000 cm^{-1}). The spectrum profile for the normal form of the *N*,*N*′-dimethylamino derivative is in a good agreement with the one presented in the work of Doroshenko et al..[8]

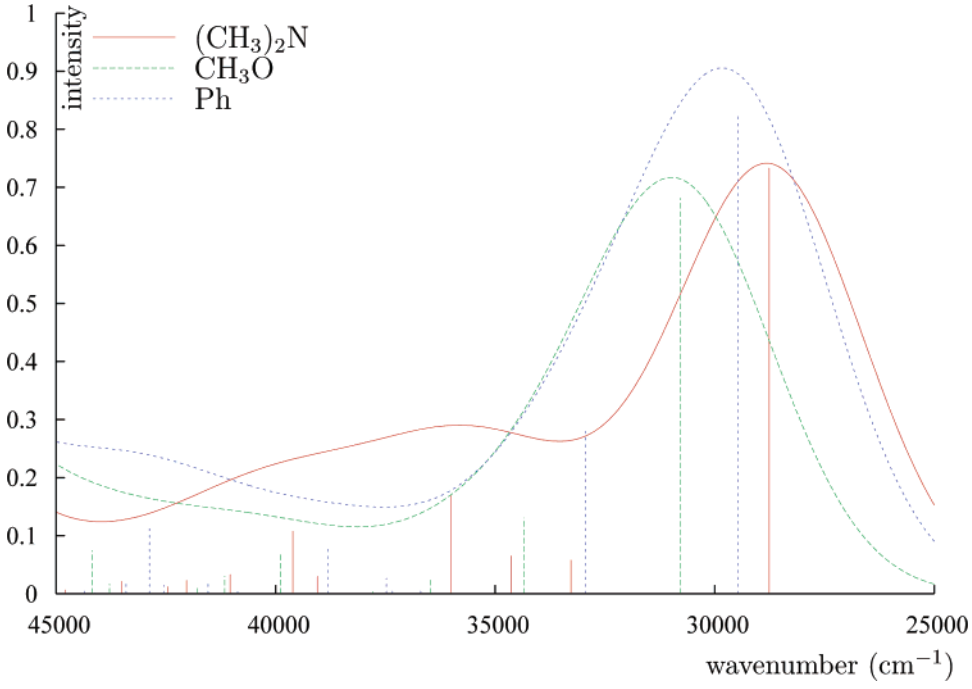

Figure 4. Calculated spectra of the normal forms.

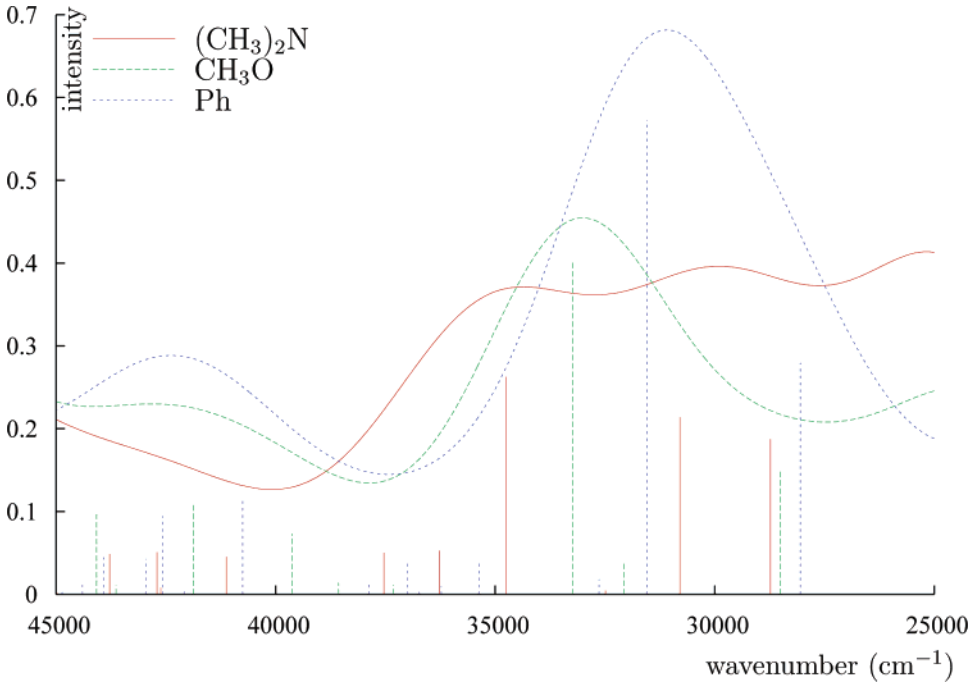

Figure 5. Calculated spectra of the tautomeric forms.

TABLE 2: Main Peaks and Stokes Shifts

	calculated (osc. strength is in parentheses)						experimental[1]				
R	ν_{abs}^{NF}	ν_{fl}^{NF}	ν_{fl}^{PT}	ν_{abs}^{PT}	$\Delta\nu^{NF}$	$\Delta\nu^{PT}$	ν_{abs}^{NF}	ν_{fl}^{NF}	ν_{fl}^{PT}	$\Delta\nu^{NF}$	$\Delta\nu^{PT}$
$(CH_3)_2N$	28760(0.73)	25718	15444	24619(0.37)	3041	13315	30200	25770	19940	4430	10260
CH_3O	30788(0.68)	27014	14474	24019(0.23)	3773	16313	31340	27600	19980	3740	11360
Ph	29464(0.82)	25090	13056	22141(0.21)	4374	16408	30860	26180	19880	2880	11160

3.3. Total Energies and Fluorescence Properties. Emission frequencies and Stokes shifts are calculated as described in section 2. Energy differences and calculated Stokes shifts are shown in Table 2 and compared to experiment.

The experimental results obtained by Doroshenko[1,8] in three solvents (octane, toluene and acetonitrile) do not show any considerable solvent effect on absorption or emission spectra of the substances under investigation. In the Table 2 we compare our results with the spectral data taken in octane. It can be seen that both absorption and emission peaks of normal forms are well reproduced by the calculations. On the other hand, the agreement between the calculated and experimentally observed emission frequencies of the phototautomeric forms is less satisfactory: the energies are underestimated by 5600 cm^{-1} on the average.

The reason for the underestimation of the S_0-S_1 energy gap of the phototautomeric forms by TDDFT is the significant contribution of an ionic structure to the PT*-S_1 wave function (that is, the involvement of a charge transfer in the transition) as suggested by high dipole moment and the nature of the orbitals involved in the transition. The TDDFT method is known to systematically underestimate excitation energies associated with molecular long-range charge transfer between an electron donor and electron acceptor and corrections require the development of correct exchange correlation functionals.[41−43] Charge-transfer excitations are predicted too low in energy by up to 1 eV. In the limit of complete charge separation, this can be related to the lack of derivative discontinuities in semi-local functionals.[44] A similar underestimation of the excitation energy has been frequently seen before,[22,38−40] especially for low-lying HOMO−LUMO excited states of large π-systems and when excited state wave function is dominated by an ionic valence-bond contribution.

3.4. Relative Stability and Reaction Rates. The reaction rate is an important characteristic of an ESIPT process. Along with the relative stability of the excited tautomeric forms, the ESIPT reaction rates determine the low- and high-wavelength fluorescence intensity ratio and the degree of fluorescence quenching. Rate constants for ESIPT processes are typically in the range $10^{10}-10^{13}$ s^{-1}.[2,8,45−48]

To obtain a qualitative estimate of the relative reaction rates, we calculated for each of the studied substance the activation barrier height for the proton-transfer reaction in the excited state by a well-known coordinate-driven minimum energy path approach,[24,35,36] According to this approach, the reaction path was modeled by stepwise moving the migrating hydrogen atom H(13) from the O(12) oxygen to the N(3) nitrogen atom. At each step we performed a constrained geometry optimization, keeping the O(12)−H(13) distance fixed and relaxing the other internal coordinates. The initial point corresponded to NF*-S_1 and the final point corresponded to PT*-S_1. The energy-versus-distance profile obtained in this way represents a cross section of the potential energy surface (PES)—a potential curve. The maximum energy point of the profile was taken as an approximation to the ESIPT transition state, and the energy difference between this highest energy point and the initial NF*-S_1 point was taken as an approximation to the activation barrier. The profiles for all the three substances are presented by Figure 6. It can be seen that the barrier of the $(CH_3)_3N$ derivative (7 kcal/mol) is appreciably higher than that of the other two derivatives (0.3−1 kcal/mol).

On the basis of several evidences suggesting the irreversibility of ESIPT processes, Doroshenko and coauthors[1,8] have consid-

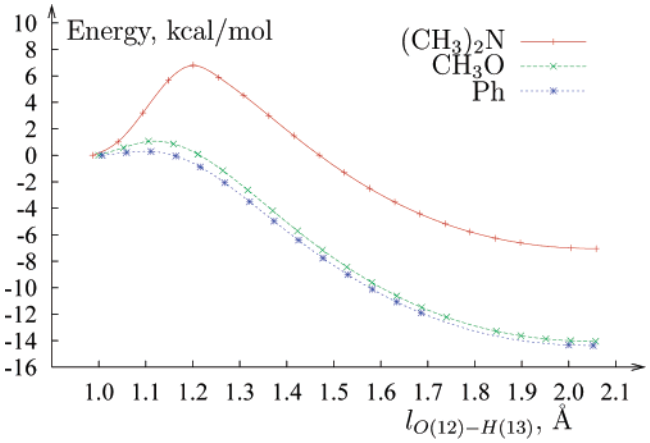

Figure 6. Potential energy curves.

TABLE 3: ESIPT Activation Barriers and Rate Constants

R	O(12)−H(13) bond length, Å	TS energy,[a] kcal/mol	k_f^{NF}	k_f^{PT}	k_{ESIPT}, s^{-1}
$(CH_3)_2N$	1.21	6.8	$3.5 \cdot 10^8$	$1.2 \cdot 10^7$	$1.9 \cdot 10^{11}$
CH_3O	1.12	1.1	$4.1 \cdot 10^8$	$8.2 \cdot 10^6$	$1.3 \cdot 10^{12}$
Ph	1.10	0.3	$4.0 \cdot 10^8$	$8.2 \cdot 10^6$	$1.4 \cdot 10^{12}$

[a] Relative to 1.

ered the generalized scheme of primary photochemical and photophysical processes that act in the excited state of any molecule capable of ESIPT. Applying the photostationarity condition, they deduced an equation relating experimentally measurable fluorescence quantum yields (ϕ_{NF} and ϕ_{PT}), and k_f (radiative), k_d (radiationless) and k_{ESIPT} (ESIPT) rate constants. Taking into account that $1/(k_f^{PT} + k_d^{PT})$ corresponds to another experimentally measurable parameter, the lifetime of the phototautomeric form τ_{PT}, they derived the following equation for k_{ESIPT}:

$$k_{ESIPT} = \frac{k_f^{NF}}{k_f^{PT}} \frac{\phi_f^{PT}}{\phi_f^{NF}} / \tau_{PT} \quad (1)$$

Following Doroshenko,[1,8] we use the values of phototautomer lifetime τ_{PT}, fluorescence quantum yields of normal and phototautomeric forms (ϕ_{NF} and ϕ_{PT}) reported in their work and estimate the radiative rate constants computationally. It is important to note that the theoretical estimation is the only way to obtain the radiative rate constant for the phototautomer (k_f^{PT}), as experimentally the phototautomeric forms do not exist in their ground states.

As suggested in the works by Doroshenko[1,8] and Aquino,[24] to estimate the values of the radiative rate constants for normal and phototautomeric forms, we utilize Einstein's spontaneous emission transition probability relation:[1,24,49]

$$k_f = \frac{f \cdot \nu^2}{1.50} \quad (2)$$

where k_f is the radiative rate constant (in s^{-1}), ν is the transition wavenumber (in cm^{-1}) and f is the corresponding oscillator strength. Calculated reaction rate constants and estimated energy barriers are presented in Table 3.

Another important property of the ESIPT-capable substances is the relative stability of the normal and tautomeric forms in the ground and excited states. In Figure 7, we schematically show energies of each form relative to the most stable one, NF-S_0. It can be seen that the normal form is more stable than

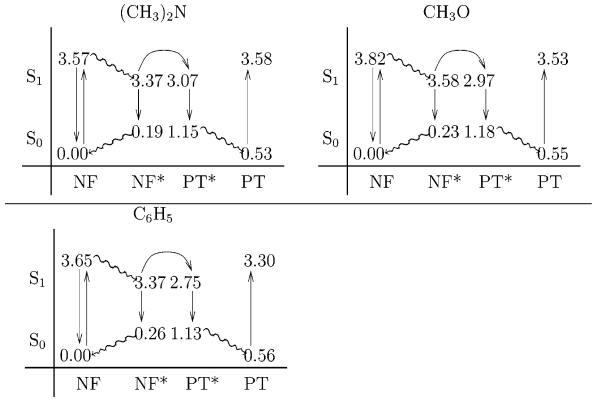

Figure 7. Energy diagrams (energies in eV).

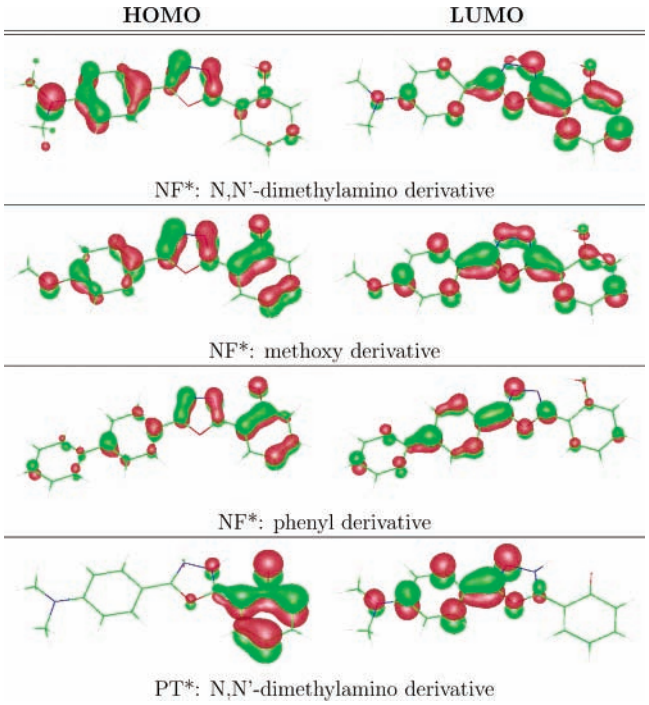

Figure 8. HOMO and LUMO of normal and phototautomeric forms.

the tautomeric form in the ground state (by 12 kcal/mol for R = $(CH_3)_2N$ and by 13 kcal/mol for the other two substituents) whereas the tautomeric form is more stable in the excited state (by 7 kcal/mol for R = $(CH_3)_2N$ and by 14 kcal/mol for the other two substituents).

Thus, the *N,N′*-dimethylamino derivative has distinctive properties compared to the other two studied compounds. Its predicted ESIPT energy barrier is considerably higher, and the energy difference between the phototautomers is less than that for the methoxy and phenyl derivatives. Apparently, the π-donating dimethylamino group stabilizes the normal form by giving electrons to the electron-accepting oxadiazole ring. The calculated ESIPT rate constant values (k_{ESIPT}) are consistent with these results. It can be concluded that electron-donating substituents in the proton-accepting part of the *o*-hydroxy-2,5-diaryl-1,3,4-oxadiazoles decrease the ESIPT reaction rate. This agrees with earlier experimental and theoretical results.[1,8]

3.5. Frontier Orbitals. The structure of the HOMO and LUMO of all three molecules are similar, but there are some quantitative differences. In all cases, both the HOMO and LUMO have π-type symmetry. General structures of HOMO and LUMO for the normal forms are shown in Figure 8.

TABLE 4: HOMO−LUMO Energies, Ionization Potentials and Electron Affinities, EV

R		HOMO	LUMO	IP	EA
$(CH_3)_2N$	NF	−5.52	−1.58	6.89	0.19
	NF*	−5.33	−1.84		
	PT*	−4.70	−2.34		
	PT	−5.20	−1.73	6.63	0.37
CH_3O	NF	−6.04	−1.78	7.45	0.36
	NF*	−5.74	−2.07		
	PT*	−4.83	−2.58		
	PT	−5.38	−1.96	6.96	0.56
Ph	NF	−6.17	−2.08	7.46	0.78
	NF*	−5.87	−2.43		
	PT*	−4.91	−2.87		
	PT	−5.46	−2.29	7.00	0.98

In the normal forms, the main contributions to HOMO are the lone pair of the hydroxyl oxygen, the C(6)−C(7) and C(9)−C(10) π-bonds, the C−N π-bonds of oxadiazole ring and, in methoxy and *N*,*N*′-dimethylamino derivatives, the lone pair of the oxygen or nitrogen atoms, respectively. It can be seen that in the dimethylamino-substituted diphenyloxadiazole, the contribution of the right phenyl ring is much less than that for the other two substances.

The LUMOs also have π-type symmetry. The main contributions to them are the N−N bond of the oxadiazole ring, the lone pair of oxygen atom of oxadiazole (O(1)) and the bonds connecting the phenyl rings with the oxadiazole fragment. The shape of the LUMO does not differ significantly between the normal forms of the three investigated molecules.

For the phototautomeric forms, the shapes of the HOMO and LUMO do not show any significant differences between the investigated molecules. The HOMO and LUMO of the dimethylamino derivative are shown in Figure 8, the pictures for the other two compounds can be found in Supporting Information.

3.6. Ionization Potentials and Electron Affinities. The ionization potential (IP) and electron affinity (EA) are important properties for organic dyes used in organic light emitting diodes (OLEDs).[12,13,50] A low ionization potential of the hole transport layer forming molecules leads to formation of exciplexes and to a decrease in OLED efficiency.[12] Thus, the electron-injecting materials should have a large electron affinity[50] and the light-emitting materials should have a small ionization potential and large electron affinity.[50] On the other hand, a small gap would result in an undesirable red shift of the electroluminescence out of visible region.[50]

We have calculated the ionization potentials and electron affinities as differences between the DFT energies of the corresponding neutral and charged radical species. The results are presented in the Table 4 along with the HOMO and LUMO energies. As expected, the ionization potential increases with the decreasing π-electron-donor ability of the substituents ($(CH_3)_2N$, CH_3O, C_6H_5).

3.7. Electron Density Redistribution. The main driving force for an ESIPT reaction is the coordinated increase of the proton-donor site acidity and the proton-acceptor site basicity in the excited state.[8] Such a change is regulated by the redistribution of the electron density in the excited state. The most straightforward way of analyzing the electron density redistribution is to study the differential density maps, but they may be difficult to formalize and interpret. Other indicators of the electron density changes are the dipole moments (principally observable) and atom charges (we have chosen to use Mulliken charge analysis).

Differential density maps are presented in Figure 9 (drawn by the gOpenMol[51,52] software; red and green colors indicate a decreased and an increased density in the excited state, respectively). The maps calculated at NF and NF* geometries do not differ by any significant extent. The same holds true also for the maps calculated at PT* and PT geometries.

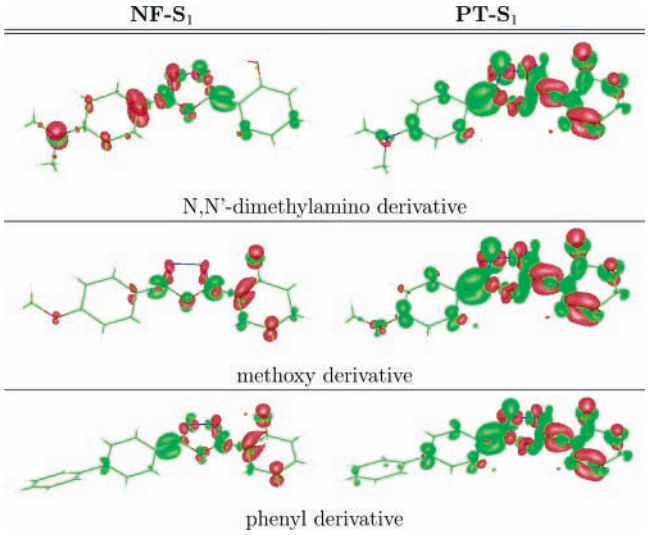

Figure 9. Differential density of NF-S_1 and PT-S_1 forms.

From the differential density maps of the first excited states of the normal forms (NF*-S_1) it can be seen that the nitrogen atom of the amino group of the *N*,*N*′-dimethylamino derivative participates in the excited state density redistribution to a considerable extent, whereas the participation of the oxygen atom of the hydroxyl group is very low. In the methoxy and phenyl derivatives the picture is the opposite: the substituent almost does not participate in the density redistribution, whereas the hydroxyl oxygen participation is significant. The amino nitrogen in the *N*,*N*′-dimethylamino derivative and hydroxyl oxygen in methoxy and phenyl derivatives are involved in the density redistribution in a similar way: they donate the density from the π-type orbitals, whereas the σ-type orbitals act as acceptors.

The differential density maps for the first exited states of the phototautomeric forms (PT*-S_1) of the molecules studied are very similar to each other, in contrast to what we observe for the normal forms. The density flows from the right to the left phenyl rings, and both the hydroxyl oxygen atom and a substituent participate in the density redistribution.

It can be concluded that for the normal forms of the methoxy and phenyl derivatives, the electron density changes both in the O(12) hydroxyl oxygen (proton-donating) atom and in the N(3) oxadiazole nitrogen (proton-accepting) atom. On the other hand, the hydroxyl oxygen atom of the dimethylamino derivative does not participate in density redistribution; therefore, one cannot expect a significant change in its acidity on the excitation. Thus, the driving force of the ESIPT reaction in this case is only the increase of the proton affinity of the N(3) oxadiazole atom. This can be a possible explanation of the lower ESIPT reaction rate and the smaller energy difference between the normal and phototautomeric forms of the dimethylamino derivative.

One can notice that in the tautomeric forms, the O(12) hydroxyl oxygen atom has a quite high negative charge ($q_{O(12)} = -0.58$ in excited state) for all three molecules which, along with positive charge of the oxadiazole ring, suggests that there is a significant contribution of the zwitterionic form in the PT*-S_1 structure. In the ground state (PT-S_0), the contribution of the zwitterionic form seems to be smaller. ($q_{O(12)} = -0.47$).

The dipole moments of the ground and excited states for both the normal and tautomeric forms of the molecules are presented

TABLE 5: Calculated Dipole Moments (Debye)[a]

R	NF-S_0	NF-S_1	NF*-S_1	PT*-S_1	PT-S_0	PT-S_1
$(CH_3)_2N$	(−)7.35	(−)17.34	(−)16.06	(+)6.89	(−)10.22	(+)4.07
CH_3O	(−)4.63	(−)3.18	(−)3.23	(+)7.19	(−)7.45	(+)6.07
Ph	(−)4.58	(+)5.95	(+)6.53	(+)10.93	(−)6.84	(+)12.18

[a] In parentheses is the sign of the dipole moment projection on C(5) → C(2) ("left−right") direction.

TABLE 6: Mulliken Atomic Charges

fragment[a]	NF-S_0	NF-S_1	NF*-S_1	NF*-S_0	PT*-S_1	PT*-S_0	PT-S_0	PT-S_1
				R = $(CH_3)_2N$				
oxa	−0.05	0.04	0.01	−0.06	0.28	0.19	0.20	0.26
N(3)	−0.14	−0.12	−0.11	−0.14	−0.09	−0.07	−0.08	−0.12
O(12)	−0.27	−0.27	−0.27	−0.27	−0.58	−0.47	−0.46	−0.54
H(13)	0.30	0.31	0.31	0.30	0.32	0.31	0.32	0.32
RPR	−0.03	0.14	0.14	−0.01	−0.52	−0.18	−0.14	−0.34
LPR	−0.09	−0.22	−0.22	−0.10	0.24	−0.03	−0.06	0.10
R	0.14	−0.00	0.02	0.14	0.26	0.18	0.15	0.20
				R = CH_3O				
oxa	−0.05	0.03	0.01	−0.05	0.29	0.20	0.20	0.25
N(3)	−0.14	−0.14	−0.14	−0.13	−0.09	−0.07	−0.08	−0.13
O(12)	−0.27	−0.32	−0.30	−0.26	−0.58	−0.47	−0.46	−0.55
H(13)	0.30	0.30	0.30	0.30	0.32	0.31	0.32	0.32
RPR	−0.02	−0.06	−0.07	−0.03	−0.51	−0.17	−0.12	−0.38
LPR	0.04	0.07	0.07	0.03	0.41	0.12	0.06	0.30
R	−0.00	−0.01	−0.01	0.00	0.07	0.01	0.01	0.05
				R = Ph				
oxa	−0.06	−0.01	0.00	−0.04	0.24	0.19	0.19	0.20
N(3)	−0.14	−0.15	−0.15	−0.13	−0.09	−0.07	−0.08	−0.12
O(12)	−0.27	−0.33	−0.31	−0.26	−0.58	−0.47	−0.46	−0.55
H(13)	0.30	0.29	0.29	0.30	0.32	0.32	0.32	0.32
RPR	−0.01	−0.16	−0.21	−0.05	−0.51	−0.17	−0.12	−0.42
LPR	0.05	0.17	0.16	0.04	0.35	0.10	0.07	0.32
R	−0.01	0.03	0.07	−0.00	0.18	0.03	0.00	0.14

[a] Legend: "Oxa" is oxadiazole ring; "RPR" is 2-phenyl ring; "LPR" is 5-phenyl ring; "R" is Substituent.

in Table 5. It can be seen that the dimethylamino derivative shows significant increase in dipole moment for the form, unlike other molecules studied here.

4. Summary and Conclusions

The geometries of the NF, NF*, PT* and PT forms of the methoxy and dimethylamino derivatives are planar, whereas those of the phenyl derivative are nonplanar with angles between the substituent phenyl ring and 5-phenyl ("left") of 39, 22, 26, and 39°, respectively. Although this hinders the π electron mobility, the σ electrons are unaffected making it a weak electron acceptor.

Absorption and emission spectra of the normal forms are in agreement with the experimental results.[8] The energy gap between the ground and excited states of the phototautomers is almost half that of the normal forms. The calculated emission frequency of the phototaumeric form is underestimated by 0.7 eV, suggesting a multideterminant picture of the phototautomeric forms (as also suggested by the two mesomeric forms in Figure 3). Energetically, the NF-S_0 form is 12−13 kcal/mol more stable than the PT-S_0 form for all three derivatives. On the other hand, the PT*-S_1 form is more stable than the NF*-S_1 form by 7 kcal/mol for the *N*,*N*′-dimethylamino and by 13 kcal/mol for the methoxy and phenyl derivatives, suggesting that the proton transfer is from NF*-S_1 to PT*-S_1. We can conclude that the equilibrium at the ground state is completely shifted toward the normal form, but in the excited state, the equilibrium is shifted toward the phototautomer.

We observe that dipole moment NF*-S_1 of dimethylamino derivative differs substantially from its NF-S_0, suggesting a considerable charge redistribution. All PT*-S_1 forms show considerable negative charge on hydroxyl oxygen and positive charge on the oxadiazole ring, suggesting a significant contribution of zwitterionic structure.

Analyzing the relative effect of substituents with different electron-donor capabilities on the proton-acceptor moiety we have found that the ESIPT rate is an order of magnitude lower (1.9×10^{11} s^{-1}) for the dimethylamino substituent than for the other studied substituents. A possible explanation to this is the low participation of the hydroxyl oxygen of the dimethylamino derivative in the density redistribution and, therefore, a smaller change in the acidity of the atom in the excited state. Stokes shifts are around 11 000 cm^{-1} for all the three derivatives. Thus, we have seen that density functional calculations can successfully be used to predict and understand the structural, electronic, and spectroscopic properties of ESIPT-capable compounds, and therefore for the design of new effective materials for OLEDs.

Supporting Information Available: Figures showing HOMOs and LUMOs of different derivatives. Tables of calculated spectral data. This material is available free of charge via the Internet at http://pubs.acs.org.

References and Notes

(1) Doroshenko, A. O.; Posokhov, E. A.; Verezubova, A. A.; Ptyagina, L. M. *J. Phys. Org. Chem.* **2000**, *13*, 253.
(2) Fahrni, C. J.; Henary, M. M.; VanDerveer, D. G. *J. Phys. Chem. A* **2002**, *106*, 7655−7663.
(3) Chou, P. T.; Martinez, M. L. *Radiat. Phys. Chem.* **1993**, *41*, 373−378.
(4) Sytnik, A.; Kasha, M. *Radiat. Phys. Chem.* **1993**, *41*, 331−349.
(5) Sytnik, A.; Valle, J. C. D. *J. Phys. Chem.* **1995**, *99*, 13028−13032.
(6) Lakowicz, J. R. *Principles of Fluorescence Spectroscopy*; Plenum Press: New York, 1983.
(7) Parthenopoulos, D. A.; McMorrow, D.; Kasha, M. *J. Phys. Chem.* **1991**, *95*, 2668−2674.
(8) Doroshenko, A. O.; Posokhov, E. A.; Verezubova, A. A.; Ptyagina, L. M.; Skripkina, V. T.; Shershukov, V. M. *Photochem. Photobiol. Sci.* **2002**, *1*, 92.
(9) Keck, J.; Kramer, H. E.; Port, H.; Hirsch, T.; Fischer, P.; Rytz, G. *J. Phys. Chem.* **1996**, *100*, 14468−14475.
(10) O'Connor, D. B.; Scott, G. W.; Coulter, D. R.; Yavrouian, A. J. *J. Phys. Chem.* **1991**, *95*, 10252−10261.
(11) Kolosov, D.; English, D. S.; Bulovic, V.; Barbara, P. F.; Forrest, S. R.; Thompson, M. E. *J. Appl. Phys.* **2001**, *90*, 3242−3247.
(12) Tamoto, N.; Adachi, C.; Nagai, K. *Chem. Mater.* **1997**, *9*, 1077−1085.
(13) Uchida, M.; Adachi, C.; Koyama, T.; Taniguchi, Y. *J. Appl. Phys.* **1999**, *86*, 1680−1687.
(14) Wang, J. F.; Jabbour, G. E.; Mash, E. A.; Anderson, J.; Zhang, Y.; Lee, P. A.; Armstrong, N. R.; N.Peyghambarian,; Kippelen, B. *Adv. Mater.* **1999**, *11*, 1266−1269.
(15) Adachi, C.; Tsutsui, T.; Saito, S. *Appl. Phys. Lett.* **1990**, *57*, 531−533.
(16) Berggren, M.; Gustafsson, G.; Ingans, O.; Andersson, M. R.; Hjertberg, T.; Wennerstrm, O. *J. Appl. Phys.* **1994**, *76*, 7530−7534.
(17) Brown, A. R.; Bradley, D. D. C.; Burroughes, J. H.; Friend, R. H.; Greenham, N. C.; Burn, P. L.; Holmes, A. B.; Kraft, A. *Appl. Phys. Lett.* **1992**, *61*, 2793−2795.
(18) Hosokawa, C.; Kawasaki, N.; Sakamoto, S.; Kusumoto, T. *Appl. Phys. Lett.* **1992**, *61*, 2503−2505.
(19) Kido, J.; Hayase, H.; Hongawa, K.; Nagai, K.; Okuyama, K. *Appl. Phys. Lett.* **1994**, *65*, 2124−2126.
(20) Antoniadis, H.; Inbasekaran, M.; Woo, E. P. *Appl. Phys. Lett.* **1998**, *73*, 3055−3057.
(21) Hu, Y.; Zhang, Y.; Wang, F. L. L.; Ma, D.; Jing, X. *Synth. Met.* **2003**, *137*, 1123−1124.
(22) Furche, F.; Ahlrichs, R. *J. Chem. Phys.* **2002**, *117*, 7433−7447.
(23) Rappoport, D.; Furche, F. *J. Am. Chem. Soc.* **2004**, *126*, 1277−1284.
(24) Aquino, A. J. A.; Lischka, H.; Hättig, C. *J. Phys. Chem. A* **2005**, *109*, 3201−3208.

(25) Sobolewski, A. L.; Domcke, W. *J. Phys. Chem. A* **2004**, *108*, 10917−10922.
(26) Treutler, O.; Ahlrichs, R. *J. Chem. Phys.* **1995**, *102*, 346−354.
(27) Becke, A. D. *J. Chem. Phys.* **1993**, *98*, 5648−5652.
(28) Becke, A. D. *Phys. Rev. A* **1988**, *38*, 3098−3100.
(29) Lee, C.; Yang, W.; Parr, R. G. *Phys. Rev. B* **1988**, *37*, 785−789.
(30) Schfer, A.; Huber, C.; Ahlrichs, R. *J. Chem. Phys.* **1994**, *100*, 5829−5835.
(31) Schfer, A.; Horn, H.; Ahlrichs, R. *J. Chem. Phys.* **1992**, *97*, 2571−2577.
(32) Weiss, H.; Ahlrichs, R.; Haeser, M. *J. Chem. Phys.* **1993**, *99*, 1262−1270.
(33) Bauernschmitt, R.; Ahlrichs, R. *J. Chem. Phys.* **1996**, *104*, 9047−9052.
(34) Bauernschmitt, R.; Ahlrichs, R. *Chem. Phys. Lett.* **1996**, *256*, 454−464.
(35) Sobolewski, A. L.; Domcke, W. *J. Phys. Chem. A* **1999**, *103*, 4494−4504.
(36) Sobolewski, A. L.; Domcke, W. *Phys. Chem. Chem. Phys.* **1999**, *1*, 3065−3072.
(37) Ahlrichs, R.; Bär, M.; Häser, M.; Horn, H.; Kölmel, C. *Chem. Phys. Lett.* **1989**, *162*, 165−169.
(38) Grimme, S.; Parac, M. *Chem. Phys. Chem.* **2003**, *4*, 292−295.
(39) Parac, M.; Grimme, S. *Chem. Phys.* **2003**, *292*, 11−21.
(40) Fabiano, E.; Sala, F. D.; Weimer, R. C. M.; Gorling, A. *J. Phys. Chem. A* **2005**, *109*, 3078−3085.
(41) Gritsenko, O.; Baerends, E. J. *J. Chem. Phys.* **2004**, *121*, 655−660.
(42) Sobolewski, A. L.; Domcke, W. *Chem. Phys.* **2003**, *294*, 73−83.
(43) Hieringer, W.; Görling, A. *Chem. Phys. Lett.* **2006**, *419*, 557−562.
(44) Dreuw, A.; Weisman, J. L.; Head-Gordon, M. *J. Chem. Phys.* **2003**, *119*, 2943−2946.
(45) Barbara, P. F.; Walsh, P. K.; Brus, L. E. *J. Phys. Chem.* **1989**, *93*, 29−34.
(46) Grabowska, A.; Sepiol, J.; Rulliere, C. *J. Phys. Chem.* **1991**, *95*, 10493−10495.
(47) Mordzinski, A. *Excited state intramolecular proton transfer: the structural and dynamic aspects*; Institute of Physical Chemistry, Polish Academy of Science: Warsawa, 1990.
(48) Chou, P.; Chen, Y.; Yu, W.; Chou, Y.; Wei, C.; Cheng, Y. *J. Phys. Chem. A* **2001**, *105*, 1731−1740.
(49) Joachain, C. J.; Brandsen, B. H. *Physics of Atoms and Molecules*; Longman Group Limited: London, 1983.
(50) Sugiyama, K.; Yoshimura, D.; Miyamae, T.; Miyazaki, T.; Ishii, H.; Ouchi, Y.; Seki, K. *J. Appl. Phys.* **1998**, *83*, 4928−4938.
(51) Laaksonen, L. *J. Mol. Graph.* **1992**, *10*, 33−34.
(52) Bergman, D. L.; Laaksonen, L.; Laaksonen, A. *J. Mol. Graph. Model.* **1997**, *15*, 301−306.